Influence of Surface Waviness for Laminar Flow Nacelle Applications

H. Medina*

Coventry University, Coventry, CV1 5FB, United Kingdom

J.M. Early†

The Queen's University of Belfast, Belfast, BT9 5AH, United Kingdom

D. Riordan‡

Bombardier Aerospace, Belfast, BT3 9DZ, United Kingdom

Transition onset over an engine nacelle is influenced by a large number of factors (for instance, surface roughness, steps, gaps and damage), many of which can be introduced as a result of the manufacturing process. Rivetting processes can lead to the introduction of surface deviations, which can be represented as either a bump or depression wave function. Previous work on the influence of leading edge roughness has demonstrated that such surface deviations can either promote or delay transition onset. The current work at Queen's University Belfast seeks to conduct a comprehensive investigation into the consequences of a depression-type surface irregularity on the transitional characteristics exhibited by a laminar flow nacelle, with specific attention paid to both the depression amplitude and streamwise location. Intial work has indicated that careful positioning of the streamwise location of the depression relative to the leading edge is critical in the selection of appropriate manufacturing tolerances, as even milliscale depressions, which have no appreciable influence on the transitional characteristics of the boundary layer, can have a significant affect on the downstream growth of the turbulent boundary layer. There is also some evidence to suggest that small depressions placed close to the leading edge can have a stabilising effect on the laminar boundary layer, leading to a delay in the transitional Reynolds number in a manner similar to that observed for subcritical protrusions.

Nomenclature

h	Amplitude of the depression (m)
l	Streamwise location of the depression (m)
L	Plate length (m)
R_c	Critical Reynolds number (transition onset)
Re	Reynolds number based on the length of the plate
R_{tr}	Transitional Reynolds number
R_x	Reynolds number based on the streamwise distance from the leading edge
u, v	Velocity components (m/s)
U_e	External velocity at the edge of the boundary layer (m/s)
U_∞	Freestream velocity (m/s)
x, y	Stream-wise and plate-normal coordinates (m)
x_{tr}	Transition onset location (m)
δ	Boundary layer thickness (m)
δ^*	Displacement thickness (m)

*Senior Lecturer, School of Mechanical and Automotive Engineering

†Lecturer, The Queen's University of Belfast, AIAA Senior Member

‡Chief Technical Engineer, Bombardier Aerospace Belfast, AIAA Senior Member

λ Wavelength of the depression (m)

I. Introduction

A. Background

Laminar flow control has been a subject of a large number of research programmes for the past 70 years, dating back to the P51 World War II programme,[1,2] and continues today to stimulate intense debate in light of the current economic trend for sustained increases in oil prices. A large body of work exists examining the problem of the laminar flow wing, considering all aspects from the natural and hybrid through the full laminar control problem,[3] but much less effort has been devoted to the problem of laminar flow over the engine nacelle, and it continues to present a significant number of challenges for the design of future configurations with enhanced laminar flow.[4–6]

In many ways, the problem of the sustainment of laminar flow over an engine nacelle is much less restrictive than the equivalent investigations on aircraft wings, as lift generation is not the primary function. Early analytical studies on the effectiveness of a natural laminar flow nacelle[7–10] indicated that a potential drag reduction of up to 2% of total aircraft drag could be achieved, without incurring a weight penalty, solely by maintaining laminar flow on an engine nacelle. This was reinforced in the NASA study by Obara[11] who indicated that the percentage drag reduction on a typical business jet configuration could be increased from 12 to 24% by extending laminar flow over all aircraft surfaces, rather than limiting efforts to the wing alone.

With these potential savings in mind, there are a number of key issues which need consideration, namely the influence of:

- Surface irregularities (such as steps, gaps, roughness, waves).
- Insect/ice accretion and damage.
- Flow conditions (Reynolds number, turbulence, angle of attack, pressure gradient, temperature gradient).
- Noise interference (engine, airframe).

In order to address some of the more fundamental issues associated with transition over engine nacelles, the current paper forms part of a validation study considering some of the issues arising due to waviness induced through the rivetting process, and how it affects both the stability of the laminar boundary layer and its subsequent influence on the location of the onset of transition to turbulent flow over engine nacelles.

Due to the complex relationship between surface profile and transition onset, the issue of leading edge roughness and its effect on the boundary layer transitional mechanisms has been of interest for many years[11–15] with the coupling between small scale leading edge imperfections and the downstream transitional mechanism long recognised. Many of the early studies indicated that roughness only served as a destabilisation mechanism, and the coupling between the roughness elements and the boundary layer instability mechanisms gave rise to a reduction in the critical Reynolds number. However, this view has been superceded in recent times, with indications that carefully positioned roughness can have a beneficial effect, with a less energetic, slower transitional process observed, and an increase in the critical Reynolds number relative to comparative 'clean' cases.[13,16–19] Subcritical roughness[17] has proven beneficial for transition control on swept wings through superharmonic disturbance forcing, and the use of distributed roughness combined with careful pressure gradient control could provide significant extensions to the percentage of the laminar flow across aerodynamic surfaces. However, the majority of this work has been conducted examining the effects of micron-sized protrusions, and much less work has been conducted considering the effects of larger scale surface imperfections and depressions.

Consequently, in an attempt to maximise the extent of laminar flow attainable over the nacelle, this work will assess the effect of a depression-type surface wave, similar to that which can arise as a result of the rivetting process, on the transitional mechanisms. Early work on the influence of rivetting on the transition process considered protruding rivet heads, but the current study considers the prescence of small scale depression arrays close to the leading edge, representative of the modern rivetting process (but also valid for small scale damage). The main objective is to establish a clear link between the geometry of the waviness profiles and the transition onset location in order to identify those geometric configurations that lead to an improved stability of the boundary layer.

II. Experimental Setup

1. General characteristics

The test programme was undertaken at low-speed wind tunnel facility at the Queen's University of Belfast. This wind tunnel has a contraction ratio of 3.2, with a rectangular cross-section $4m$ long, $1.2m$ wide and $0.84m$ tall. Three screens have been installed to help reduce the turbulence intensity at the test section; two are located upstream of the test section within the settling chamber and the remaining screen is located in the lower section of the wind tunnel and downstream from the driving fan. The maximum operating speed with all screens installed is approximately $25m/s$. The turbulence intensity in the wind tunnel with the experimental rig in place is shown in Figure 1.

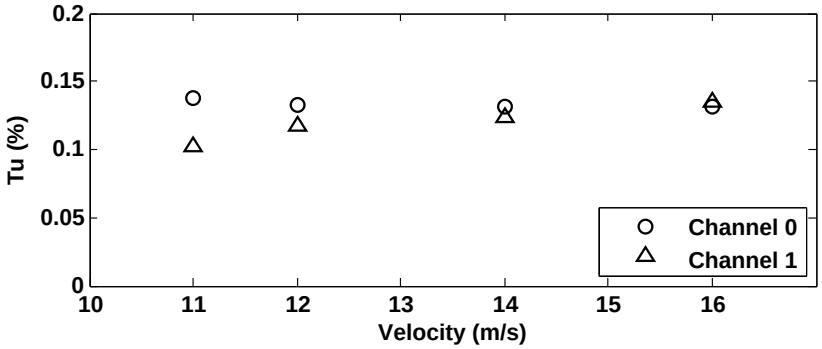

Figure 1. Free-stream turbulence intensity 0.3m from model surface at leading edge

A reconfigurable experimental rig was specifically developed for the test series (Figures 2,3). This rig consists of three separate insert plates, a trailing edge flap in order to control the location of the stagnation point on the leading edge and a removable leading edge section. A number of pressure tappings are located streamwise along the plate sections, with an additional 10 pressure tapping located within the wave profiles themselves. The two hot wire probes used for the survey (discussed in more detail below) are automated for both streamwise and vertical increments, with spanwise adjustments undertaken manually. In order to account for interference effects, the probes were offset from the tunnel centreline by $90x10^{-3}m$.

Figure 4 depicts the matching between the experimental rig and a computational Blausius profile under zero pressure gradient, which indicates an excellent agreement.

The geometry used to model the surface waviness consists of a flat plate with an imposed cosine bell function (Figure 5). The waviness profiles are defined using a given amplitude (h) and wavelength (λ), which are located at a given distance from the leading edge (l). The function used is shown in Equation 1.

$$y = h(\frac{\cos(\frac{2\pi x}{\lambda}) - 1}{2}) \tag{1}$$

2. Temperature drift

The 2D map of the velocity distribution over the test model was generated using hot-wire anemometry. While the technique has a large number of advantages and is widely used for boundary layer surveys, the large time period over which data ia recorded can have significant consequences for the temperature profile in the working section (for the current study, runtime was approximately 4.5 hours for a single 2D velocity map). Several tests were carried out to assess the temperature increase for different operating velocities, and it was found that when the wind tunnel operates at velocities equal to or higher than $16m/s$, the rate of increase of temperature was significantly higher - up to $5°C$ in some cases during the 4.5 hour acquisition window. Therefore, $14m/s$ was selected as the maximum operating velocity, at which velocity increases of approximately $3.5°C$ were observed.

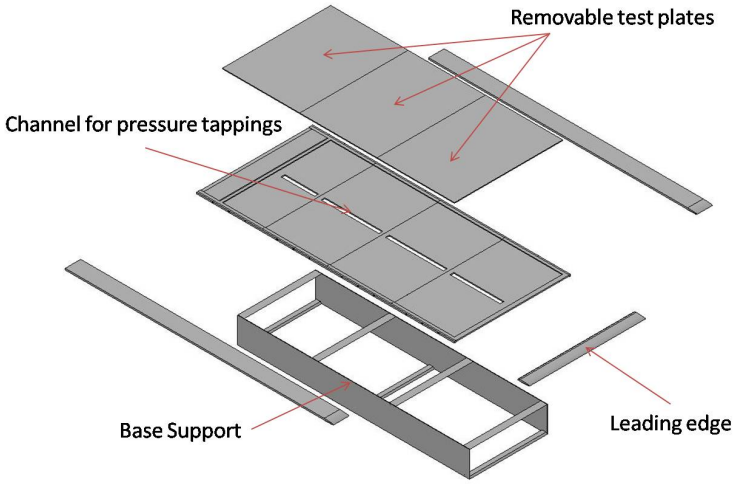

Figure 2. Experimental configuration (exploded view)

Figure 3. Experimental configuration (installed)

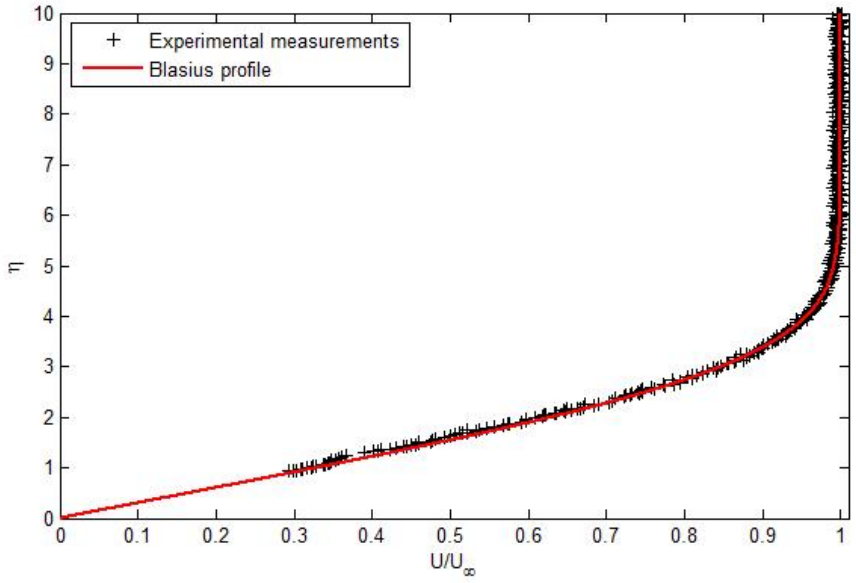

Figure 4. Comparison of experimental data and theoretical velocity profiles

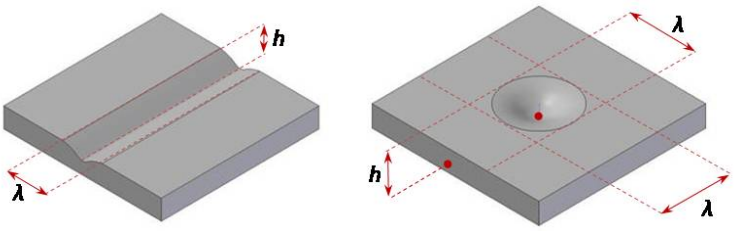

Figure 5. Schematic of Channel and Depression models tested

A. Hot wire anemometer

1. *Specification*

The velocity measurements presented were obtained using the AN-1005 hot wire and hot film Anemometry System manufactured by A.A LAB SYSTEMS LTD. This system is capable of measuring 4 channels at 16-bit resolution at a sampling rate of $500KHz$. It also offers two bridge ratios, namely, 1:1 and 1:10, as well as integrated signal conditioning (voltage offset and gain) and cable resistance compensation for calibration. It also incorporates a pulse generator to adjust the pulse response of each channel and their sensors. The over-heat ratio of the sensor can be manually adjusted by changing the decade resistance. With all these features as standard, the process of balancing the Whetstone bridge is both highly accurate and relatively simple.

2. *Probes*

Two channels were used during the acquisition process in order to generate 2 different velocity maps at equal distance from the centreline of the test model to monitor the flow for any potential anomalies. Two different probes were used during the experiments. A miniature tungsten probe from Dantec Dynamics (55P15) with a wire diameter of $5x10^{-6}m$ and a length of $1.25x10^{-3}m$ was used due to its response in low and high turbulence environments, and a gold plated probe (also manufactured by Dantec Dynamics (55P05)) with the same diameter, but with a length of $3x10^{-3}m$ due to its effective repose at low turbulence intensities.

B. Data acquisition card

A National Instruments PCI-6035E acquisition card was used to provide an interface between the anemometer and the PC in order to store the data for post-processing. This card has an A/D converter with a 16 bit resolution and provides input for 16 analog channels at a maximum sampling rate of $200KHz$. The input range can be within $\pm 0.05V$ to $\pm 10V$. During the tests presented, the input range was set to $\pm 5V$ in order to obtain the highest resolution possible without the need to use signal conditioning, other than the frequency cut-off filter.

C. Traverse system

An automated two-axis traverse system was developed in order to reduce the time needed to complete the tests and to ensure the accurate positioning of the probes. The streamwise axis (longitudinal direction) was controlled using an isel Microstep Controller (C-142-4.1) providing a signal to drive the motor with 2000 steps per revolution ($1mm$ displacement), giving an accuracy of $5x10^{-4}m$. The vertical axis (perpendicular to the test plate) was controlled using a Parker PDFX ministep indexer-driver. The motor has a resolution of 4000 steps per revolution which leads to a linear displacement of $2mm$, giving a positioning accuracy of $5x10^{-4}m$.

1. *Temperature correction*

Due to the long duration of the tests, the temperature within the wind tunnel increased during the tests (as described in section 2). Therefore, the temperature at which the sensor was calibrated and that of the medium at the time of acquisition differed.

In order to correct the voltages, the Bearman[20] correction was used (Equation 2):

$$E_{corr} = \left(\frac{T_w - T_0}{T_w - T_a}\right)^m E_a \tag{2}$$

Where E_{corr} is the corrected voltage and E_a is the acquired voltage. T_w, T_0 and T_a correspond to the sensor hot temperature, the ambient reference temperature and the ambient temperature during acquisition. Finally m is a correction exponent typically within 0.5 and 0.65. This expression can be used for moderate temperature changes in air ($\pm 5°C$), which is within the temperature changes observed during each test. As the current test programme indicated changes in temperature of $\approx 3.5^{(\circ)}C$), this correction is suitable.

2. Calibration

The hot wires were calibrated in situ at $0.15m$ below the wind tunnel pitot tube in order to prevent flow interferences. For each calibration point, the temperature was also recorded with appropriate corrections made using Equation 2. A 4^{th} order polynomial data fit was used.

3. Error and uncertainly

The estimated error associated with the different turbulent quantities is shown in Table 1.

Quantity	**Error**
U	1%
u'	2.2%
u'^2	3.4%
u'^3	6.7%

Table 1. Estimated errors

III. Base flow and experimental validation

In order to ensure that all features imparted to the flow as a result of the inclusion of the surface depression could be fully extracted, a survey of the base flow across a flat plate was undertaken. As would be expected, there is a slight decrease in R_{tr} as the Reynolds number is increased, with the corresponding decrease in thickness of the laminar region of the boundary layer (Figure 6). The corresponding normal Reynolds stress, u'^2/U^2, in the streamwise direction are also shown. As the free-stream Reynolds number is increased from $Re = 1.4x10^6$ to $1.8x10^6$, the location of the onset of transition to turbulent flow decreases from $Rx = 6.25x10^5$ to $5.9x10^5$. It also confirms that as the Reynolds number is increased, the physical distance over which the transition process takes place is reduced. The increase of the Reynolds stress over the transitional region is a consequence of the momentum exchange taking place as the velocity profiles become 'fuller' and can be responsible for the increase in drag associated with boundary layer transition.

There is an excellent correlation for the momentum thickness between the experimental and the computational results obtained from a Linear Stability Theory calculation for the two lower Reynolds number range (Figure 7). However, once the Reynolds number increased to $Re = 1.7x10^6$, the model over-estimates the growth rate of the momentum thickness over the turbulent region of the flow. This discrepancy is the result of the threshold used to close the computation iterations for the turbulent profiles. The limit to close the iterations was adjusted when the LST model was developed using published data for the momentum thickness growth over flat plates. However, the current setting is considered to be the best approximation possible, considering that the turbulent region of boundary layer flow is no longer two dimensional and the LST model is limited to two dimensional flows. Nonetheless, the correlation of the experimental data and the computational results over the laminar region of the boundary layer is excellent.

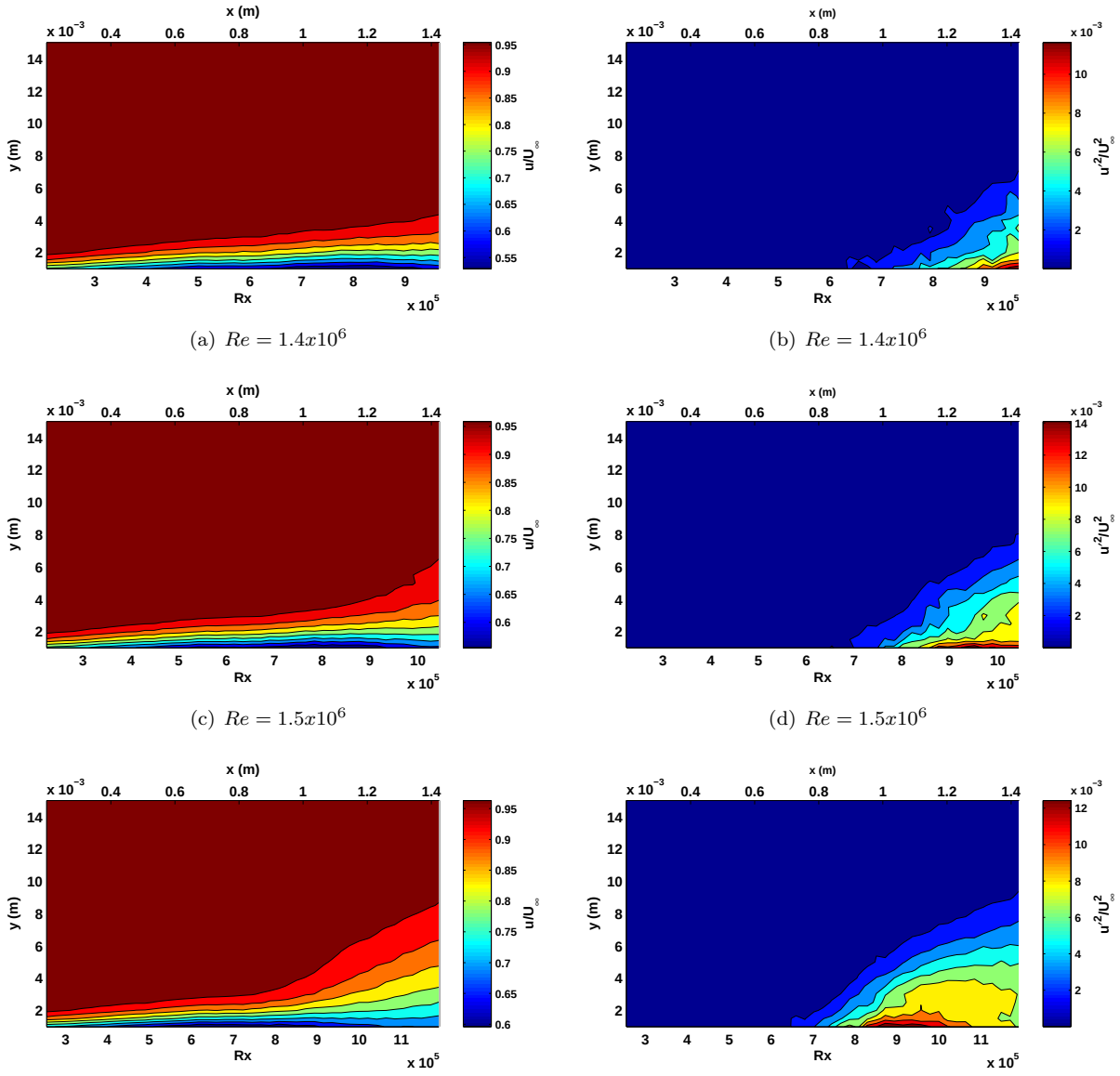

(a) $Re = 1.4x10^6$

(b) $Re = 1.4x10^6$

(c) $Re = 1.5x10^6$

(d) $Re = 1.5x10^6$

(e) $Re = 1.7x10^6$

(f) $Re = 1.7x10^6$

Figure 6. Flow over a flat plate at zero pressure gradient: Mean flow (left-hand side), Reynolds stress (right-hand side)

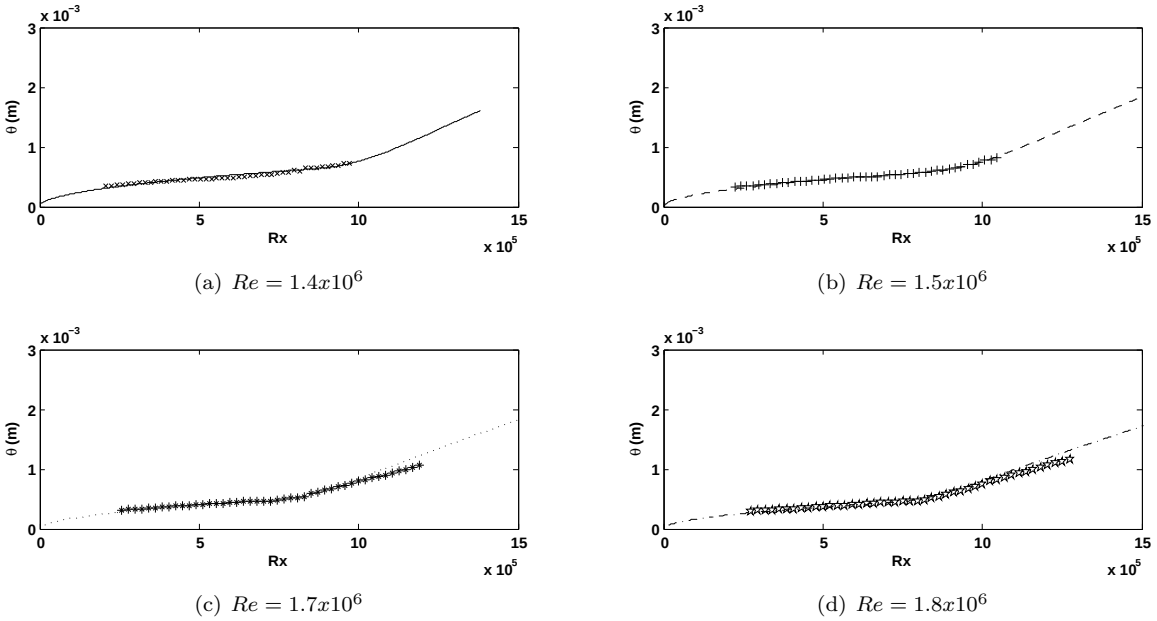

(a) $Re = 1.4x10^6$ (b) $Re = 1.5x10^6$

(c) $Re = 1.7x10^6$ (d) $Re = 1.8x10^6$

Figure 7. Validation: Momentum thickness (*** experiment, − − − computation)**

IV. Two-Dimensional Channel

Once the flow across the flat plate was validated, a range of tests were undertaken to first understand the effects of a 2D depression channel on the transitional behaviour. This was sub-divided into two main themes - the effect of varying amplitude, and the effect of streamwise location.

Re	$h(m)$	$l(m)$	$\lambda(m)$
$1.4x10^6$	$0.31x10^{-3}$	$213.74x10^{-3)}$	$63.5x10^{-3}$
$1.4x10^6$	$0.63x10^{-3}$	$213.74x10^{-3)}$	$63.5x10^{-3}$
$1.4x10^6$	$1.27x10^{-3}$	$213.74x10^{-3)}$	$63.5x10^{-3}$

Table 2. Summary of presented scaled amplitude cases (2D/3D)

Re	$h(m)$	$l(m)$	$\lambda(m)$
$1.4x10^6$	$0.63x10^{-3}$	$213.74x10^{-3}$	$63.5x10^{-3}$
$1.4x10^6$	$0.63x10^{-3}$	$463x10^{-3}$	$63.5x10^{-3}$
$1.4x10^6$	$0.63x10^{-3}$	$547x10^{-3}$	$63.5x10^{-3}$
$1.5x10^6$	$0.63x10^{-3}$	$213.74x10^{-3}$	$63.5x10^{-3}$
$1.5x10^6$	$0.63x10^{-3}$	$463x10^{-3}$	$63.5x10^{-3}$
$1.5x10^6$	$0.63x10^{-3}$	$547x10^{-3}$	$63.5x10^{-3}$

Table 3. Summary of presented scaled streamwise cases (2D/3D)

A. Effect of the amplitude (h)

This section presents the effect of the amplitude of the depression profile on the development of the boundary layer. In order to isolate the effects of the amplitude alone, all other parameters were held constant. The free-stream Reynolds number was kept equal to $Re = 1.4x10^6$, and the streamwise location of the depression and the wavelength were fixed at $l = 213.74^{-3}m$ and $\lambda = 63.5x10^{-3}m$ respectively. Three scaled amplitudes

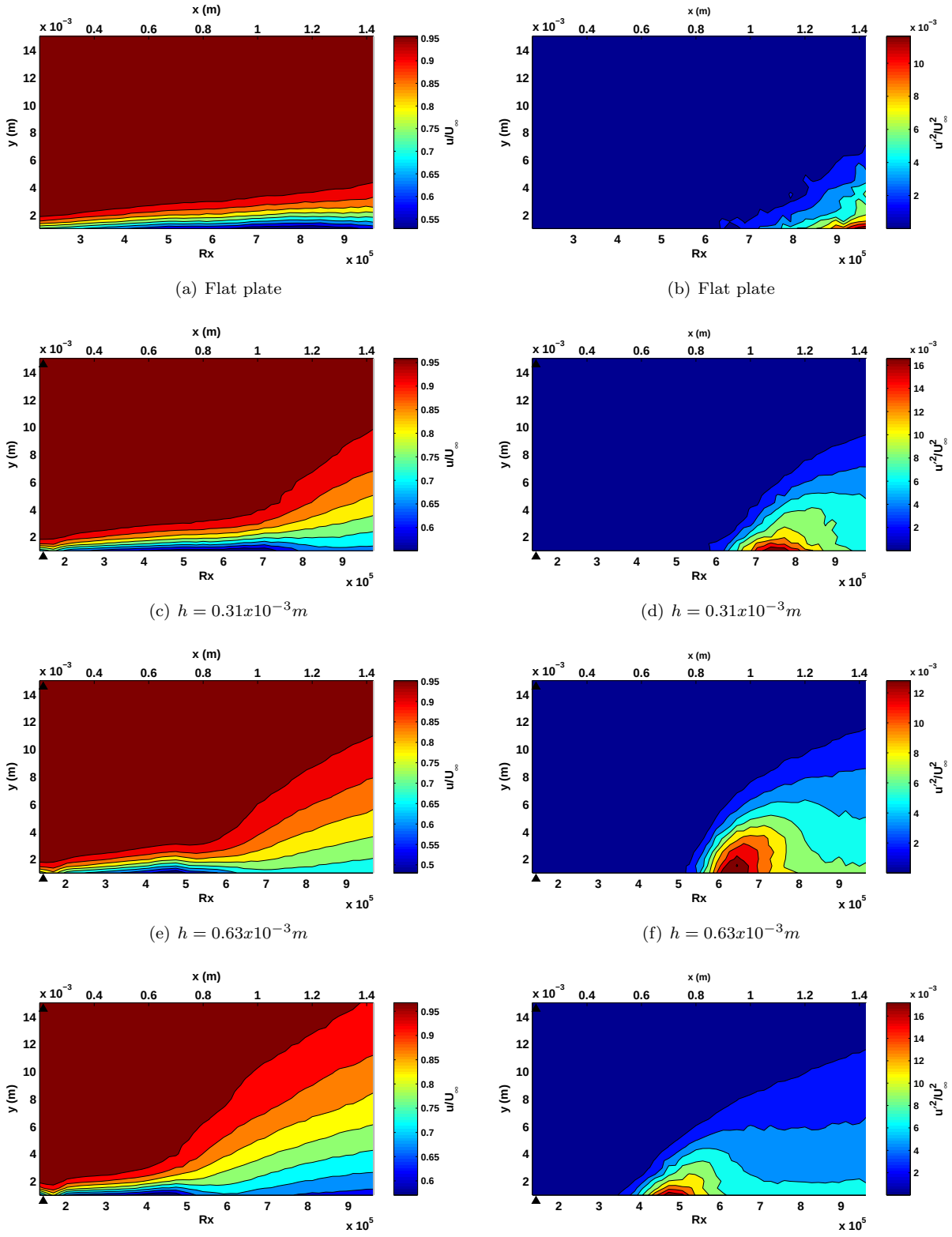

(a) Flat plate

(b) Flat plate

(c) $h = 0.31x10^{-3}m$

(d) $h = 0.31x10^{-3}m$

(e) $h = 0.63x10^{-3}m$

(f) $h = 0.63x10^{-3}m$

(g) $h = 1.27x10^{-3}m$

(h) $h = 1.27x10^{-3}m$

Figure 8. Effect of the amplitude of 2D depressions and baseline flow ($Re = 1.4x10^6$): Mean flow (left-hand side), Reynolds stress (right-hand side), depression location indicated

are presented: $0.31x10^{-3}m$, $1.27x10^{-3}m$ and $h = 1.27x10^{-3}m$.

For the cases examined, a pronounced effect of the depression on the flow field is obvious, particularly on the development of the downstream turbulent boundary layer (Figure 8).

While the depression amplitude exhibits a negligible effect on the thickness of the laminar boundary layer, it does have a significant effect on the development of the turbulent boundary layer and the critical Reynolds number. As the amplitude of the depression is increased, there is a marked decrease in the local Reynolds number (R_x) where the boundary layer begins to grow - when the amplitude of the depression is increased from $h = 0.31x10^{-3}m$ to $h = 1.27x10^{-3}m$, the local Reynolds number of the onset of turbulent boundary layer growth decreases from $R_x = 8x10^5$ to $R_x = 4x10^5$ (Figure 13a). There is a clear indication of the linear nature of the relationship between the onset of transition and the height of the 2D depression. Increasing the amplitude of the depression also leads to a significant increase in the turbulent boundary layer thickness for equivalent values of R_x (compare the turbulent growth shown in Figure 8c with Figure 8g).

Interestingly, for the case when $h = 0.31x10^{-3}m$, the critical Reynolds number is similar to that of the flat plate. However, the turbulent boundary layer growth is much more rapid in the presence of the depression channel, and the boundary layer transition from the laminar to the turbulent flow regime occurs in a shorter distance. This can be most clearly seen comparing figures 8b and 8f, which show the distribution of the Reynolds stress for the flat plate and the plate with a depression profile respectively.

B. Effect of the streamwise location (l)

The effect of the streamwise location (l) from the leading edge of the depression profile on the distribution of the mean velocity and Reynolds stress is shown in Figure 9. There is a significant effect on the overall flow field due to the modification of l and the development of the boundary layer, but the nature of the relationship is much more complex than that observed for varying the amplitude. By increasing the distance from the leading edge from $l = 213x10^{-3}m$ to $l = 463x10^{-3}m$, the region of laminar flow achieved over the flat plate is significantly increased (although it should be noted that there is no appreciable influence on the laminar boundary layer thickness), with a corresponding reduction in the transitional length. However, a further increase to $l = 547x10^{-3}m$ results in a reduction in the critical Reynolds number based on Reynolds stress. This would indicate that while a positive effect can be obtained by moving the depression element further downstream, there is a critical limit beyond which the element begins to have a destabilising effect again (Figure 13b). The reason behind this decrease in the critical Reynolds number is not currently understood and requires further investigation.

V. Three-Dimensional Array Elements

As the depressions encountered in real manufacturing environments tend to be three-dimensional in nature, the study was further extended to include the influence of a three-dimensional depression array element on the transitional behaviour. The 3D depressions were modelled as fully symmetric (Figure 5. The test conditions for the two-dimensional channels were replicated, with both amplitude and streamwise location re-assessed for comparison (refer to Tables 2 and 3).

A. Effect of the amplitude (h)

Figures 10 shows the flow field over a flat plate in the presence of 3D depression array element. First of note is that the effect of the 3D depressions on the mean flow is not a pronounced as 'equivalent' 2D depressions (compare to Figure 8), demonstrating that the flow is less sensitive to the prescence of 3D rathern than 2D depressions. The mean flow across the surface is very similar to that observed across the clean plate case, and onset of transition (based on Reynolds stress) is roughly equivalent for the two larger amplitude cases. However, an interesting effect was noted for the smallest depression amplitude tested. When the 3D depression amplitude was further decreased to $h = 0.31x10^{-3}m$, an increase in the onset location was observed, to $Rx \approx 7.5x10^5$, which is slightly higher than that achieved for the clean plate cases (Figure 13a). What becomes immediately obvious from this is the non-linear nature of the relationship between the 3D depression amplitude and the onset of transition, in comparison with the flow observed for the equivalent boundary layer development over the 2D channel.

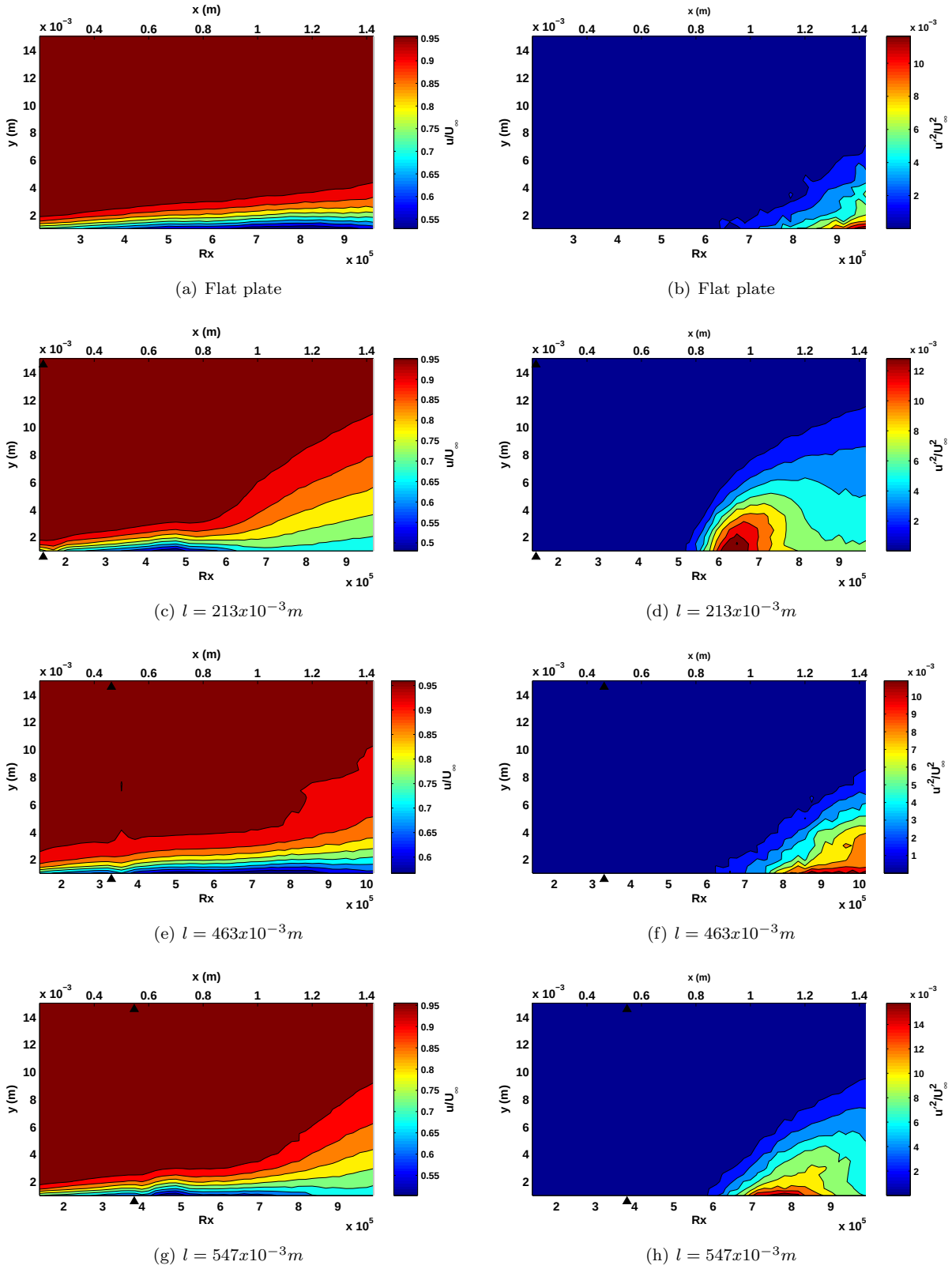

(a) Flat plate

(b) Flat plate

(c) $l = 213x10^{-3}m$

(d) $l = 213x10^{-3}m$

(e) $l = 463x10^{-3}m$

(f) $l = 463x10^{-3}m$

(g) $l = 547x10^{-3}m$

(h) $l = 547x10^{-3}m$

Figure 9. Effect of the streamwise location of 2D depressions and baseline flow ($Re = 1.4x10^6$): Mean flow (left-hand side), Reynolds stress (right-hand side)

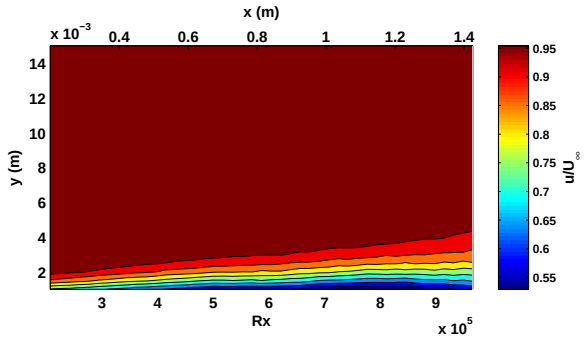

(a) Flat plate

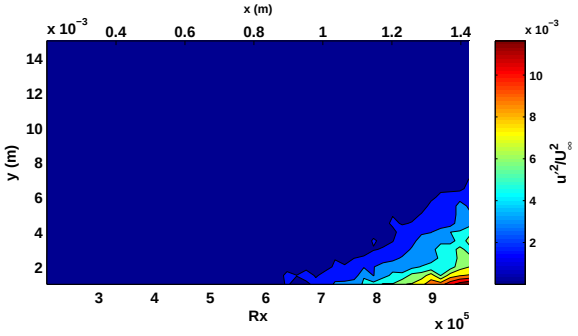

(b) Flat plate

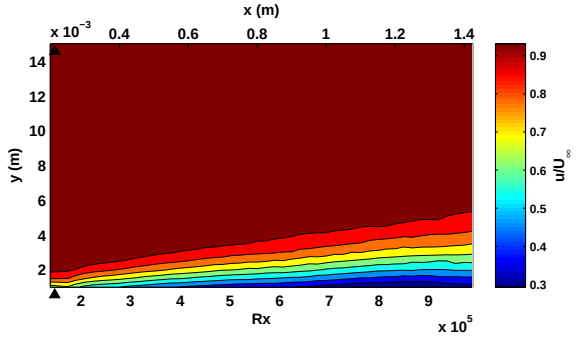

(c) $h = 0.31x10^{-3}m$

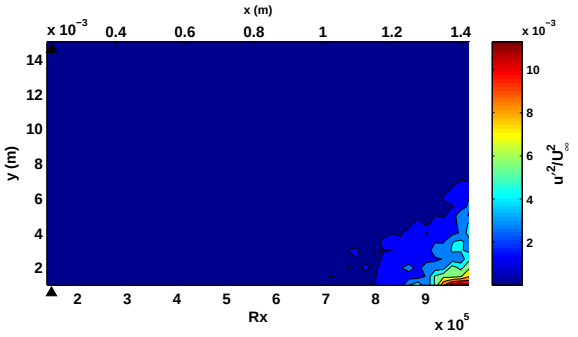

(d) $h = 0.31x10^{-3}m$

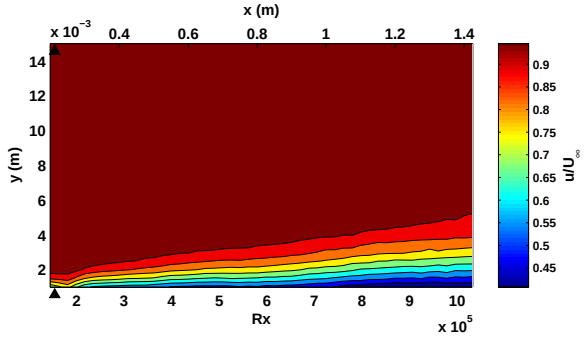

(e) $h = 0.63x10^{-3}m$

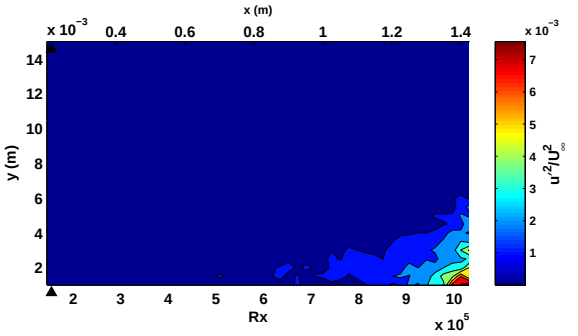

(f) $h = 0.63x10^{-3}m$

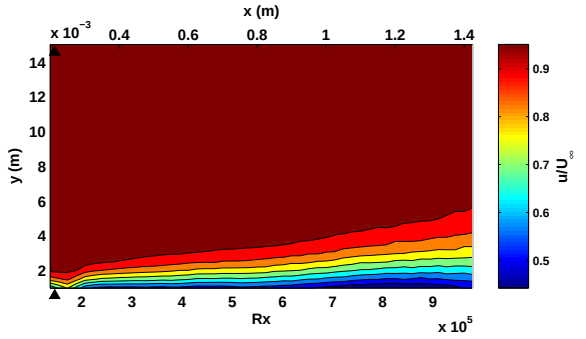

(g) $h = 1.27x10^{-3}m$

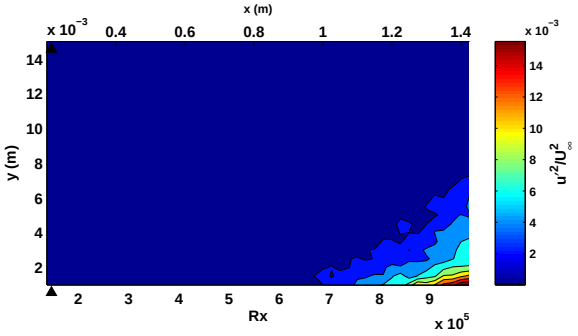

(h) $h = 1.27x10^{-3}m$

Figure 10. Effect of the amplitude of 3D depressions and baseline flow ($Re = 1.4x10^6$): Mean flow (left-hand side), Reynolds stress (right-hand side)

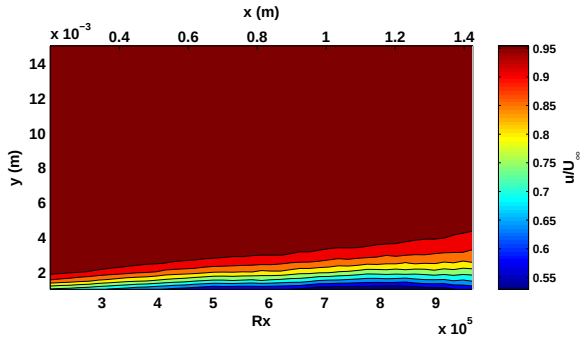

(a) Flat plate, $Re = 1.4x10^6$

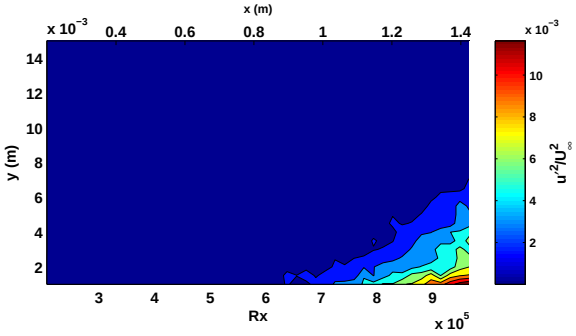

(b) Flat plate, $Re = 1.4x10^6$

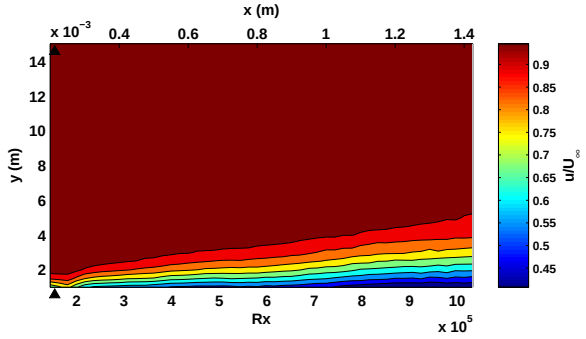

(c) $l = 213x10^{-3}m$, $Re = 1.4x10^6$

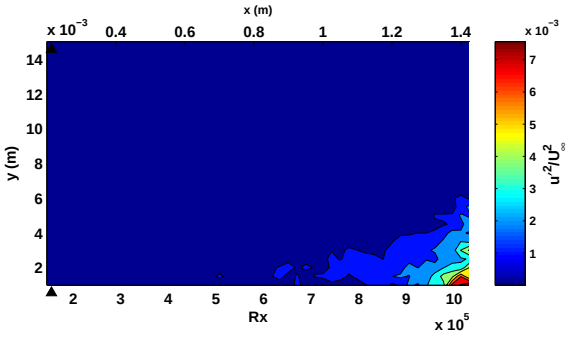

(d) $l = 213x10^{-3}m$, $Re = 1.4x10^6$

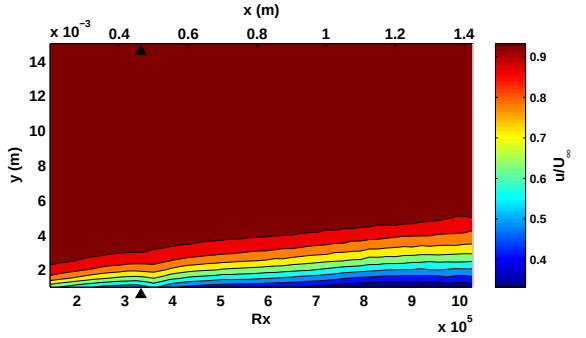

(e) $l = 463x10^{-3}m$, $Re = 1.4x10^6$

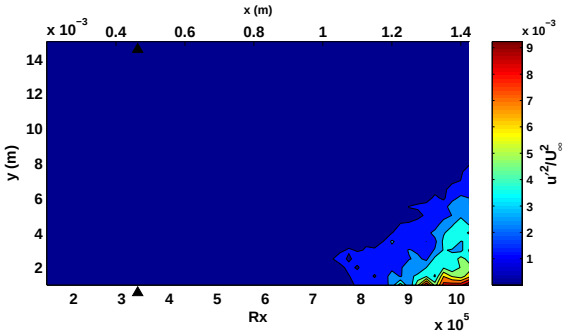

(f) $l = 463x10^{-3}m$, $Re = 1.4x10^6$

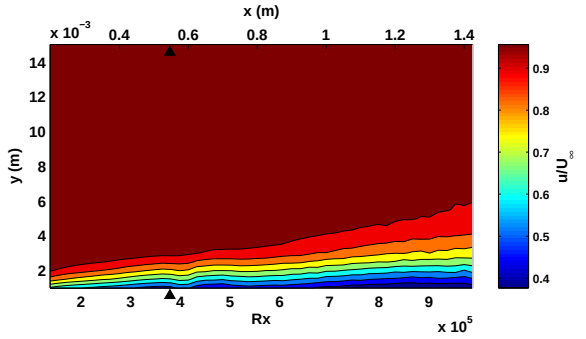

(g) $l = 547x10^{-3}m$, $Re = 1.4x10^6$

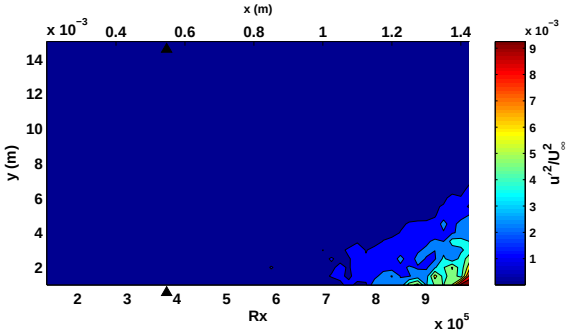

(h) $l = 547x10^{-3}m$, $Re = 1.4x10^6$

Figure 11. Effect of the streamwise location of 3D depressions, $Re = 1.4x10^6$: Mean flow (left-hand side), Reynolds stress (right-hand side)

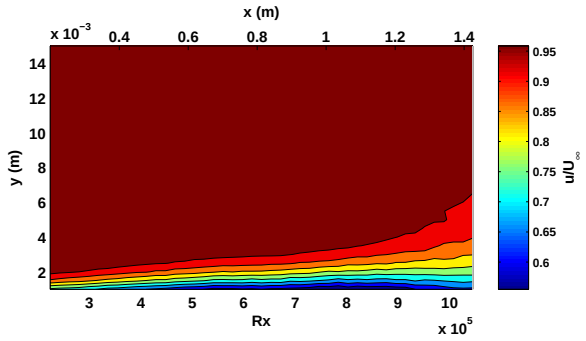

(a) Flat plate, $Re = 1.5x10^6$

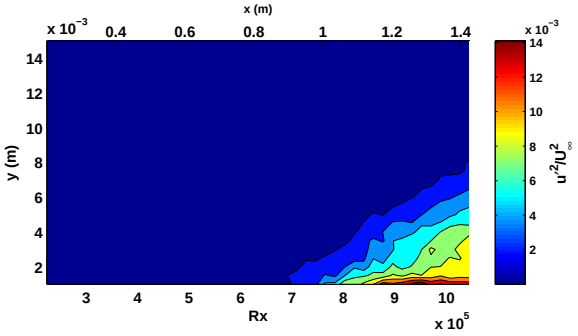

(b) Flat plate, $Re = 1.5x10^6$

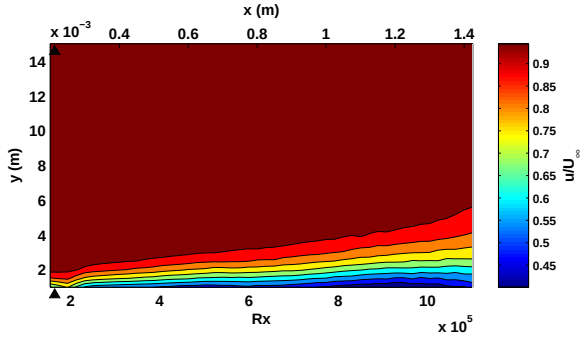

(c) $l = 213x10^{-3}m$, $Re = 1.5x10^6$

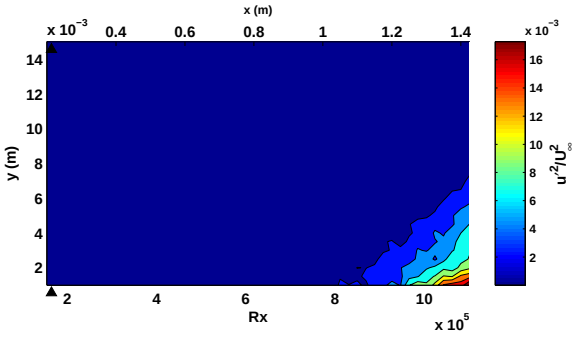

(d) $l = 213x10^{-3}m$, $Re = 1.5x10^6$

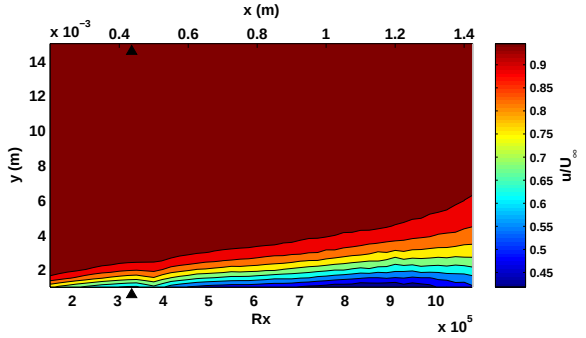

(e) $l = 463x10^{-3}m$, $Re = 1.5x10^6$

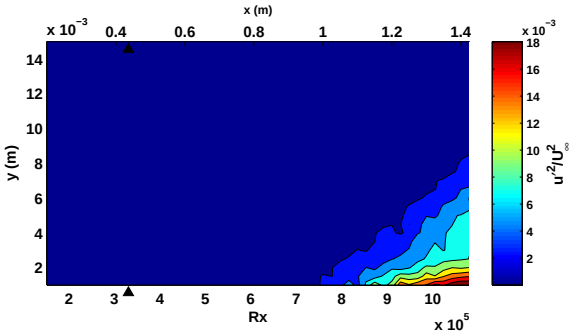

(f) $l = 463x10^{-3}m$, $Re = 1.5x10^6$

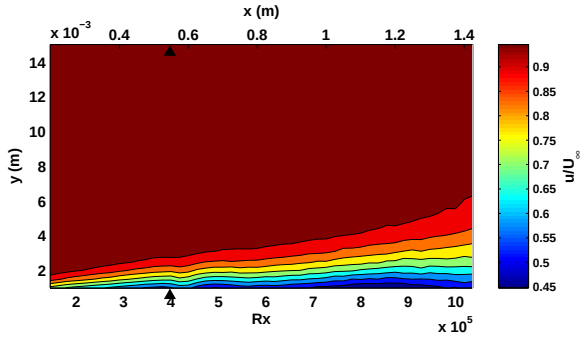

(g) $l = 547x10^{-3}m$, $Re = 1.5x10^6$

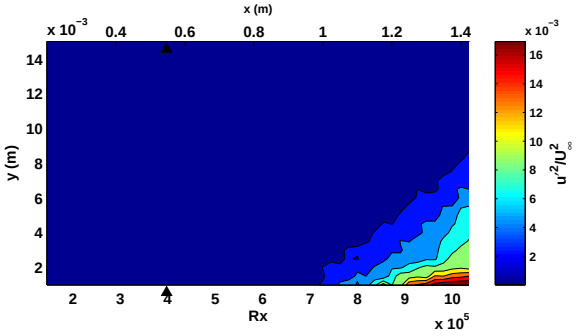

(h) $l = 547x10^{-3}m$, $Re = 1.5x10^6$

Figure 12. Effect of the streamwise location of 3D depressions, $Re = 1.5x10^6$: Mean flow (left-hand side), Reynolds stress (right-hand side)

B. Effect of the streamwise location (l)

The first thing of note when examining the influence of the streamwise location of the three-dimensional depressions (Figure 11) is that the stability of the boundary layer is less sensitive to the location of 3D depressions than to the streamwise location of 'equivalent' 2D channel profiles (as shown in Figure 9). Consequently, the streamwise location of 3D depressions does not influence the value of the critical Reynolds number as markedly as 2D depressions.

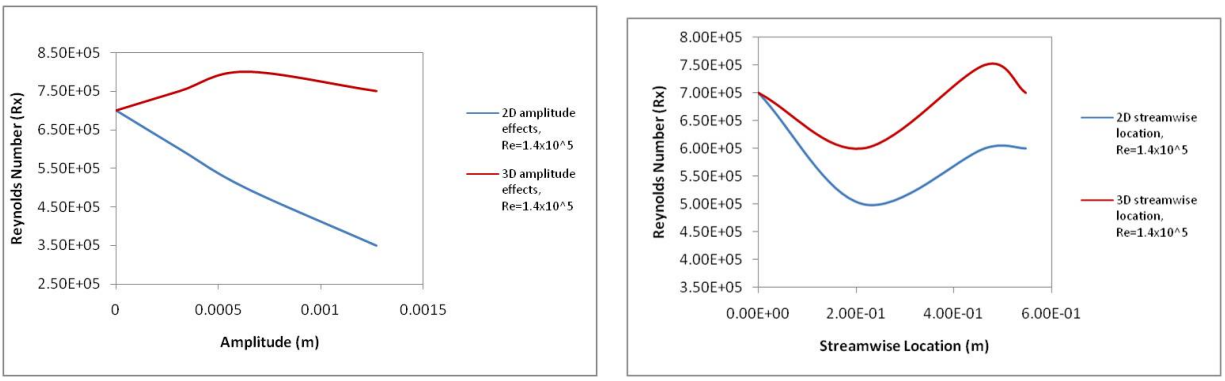

(a) Summary of Amplitude Effects (2D/3D)

(b) Summary of Streamwise Location Effects (2D/3D)

Figure 13. Summary of the effect of amplitude and streamwise location on transition Reynolds number

Nonetheless, the location of 3D depressions still has a significant affect on the flow. For instance, for $Re = 1.4x10^6$, shifting the depression from $l = 213x10^{-3}m$ to $l = 463x10^{-3}m$ increases the onset of transition from $Rx \approx 6x10^5$ to $Rx \approx 7.5x10^5$. However, when the depression is moved further downstream to $l = 547.08x10^{-3}m$ the onset of transition decreases to $Re \approx 7x10^5$ (again indicative of the prescence of a limit, as observed for the two-dimensional profiles, and the similarity in the trend can be observed in Figure 13b). It is interesting to note that for $Re = 1.4x10^6$, the onset of transition for both depressions located at $l = 463x10^{-3}m$ and $l = 547x10^{-3}m$ occurs further downstream when compared to the flat plate case (Figure 11g).

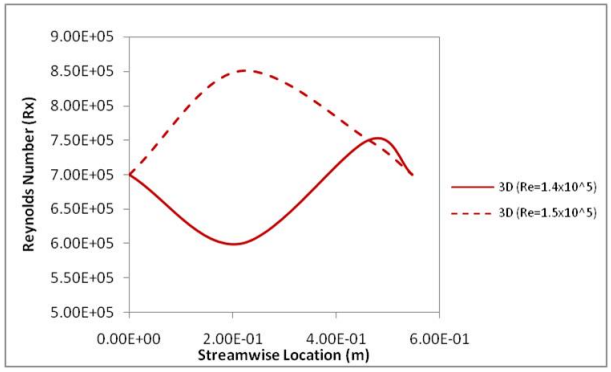

Figure 14. Summary of the effect of Freestream Reynolds number on transition Reynolds number

So far it has become apparent that both the nature (2D or 3D) and the geometrical characteristics (amplitude and streamwise location) of the depressions affect the location of the onset of transition to some degree. Another interesting effect worth mentioning is that in the presence of both 2D and 3D depressions, the free stream Reynolds number also affects the location of the onset of transition. For instance figure 12d shows that as the Reynolds number increases from $Re = 1.4x10^6$ to $Re = 1.5x10^6$ ($l = 213x10^{-3}m$, $h = 0.63x10{-}3m$), the onset of transition also increases from $Rx \approx 6x10^5$ to $Rx \approx 8.25x10^5$ (Figure 14). If the streamwise location of the depression relative to the leading edge is then increased, the location of the onset of transition decreases. This observation may appear counter-intuitive, but may be attributed to the complex interaction between instability mechanisms and the surface waviness profile. This interaction is not

currently fully understood and deserves further investigation.

VI. Conclusions

The effect of 2D channel and 3D depression profiles on the development of the boundary layer over a flat plate at zero pressure gradient were examined. The objective of this work was to assess the influence that such geometrical perturbations have on the transition of the boundary layer for laminar flow nacelle applications. For this purpose, the 2D and 3D profiles were selected to represent surface irregularities which may arise as a result of typical manufacturing processes such as rivetting. Firstly, it was found that, in general, the presence of 2D surface irregularities leads to a significant reduction on the extent of laminar flow in comparison to the flow over a flat plate. In addition, the transitional Reynolds number is extremely sensitive to both the amplitude and the streamwise location of a 2D irregularity. In contrast, the amplitude and the streamwise location of 3D depressions were found to have a less pronounced effect of the development of the boundary layer and the subsequent transitional Reynolds number. In fact, for the amplitudes and streamwise locations tested, the development of the boundary layer over 3D depressions is similar to that over a flat plate, but that the laminar boundary layer is thicker in the presence of 3D depressions. Finally, under certain combinations of the amplitude and the location of 3D depressions, it was found that the attainable region of laminar flow can be extended compared to the flat plate case. However, the extent of laminar flow for 3D depression is dependent on the complex relationship between the effects of its amplitude and its location. This complex relationship is attributed to the dampening effect that the depressions can incur on the TS waves under certain conditions. At present such effect is not fully understood and it deserves further study, in particular due to the potential to use this knowledge to systematically extend the region of laminar flow over engine nacelles by purposefully reducing the tolerance of rivets, and by carefully placing such rivets so that the end result is an extended region of laminar flow over the nacelle.

Acknowledgements

This project was co-funded by the Technology Strategy Board's Collaborative Research and Development programme, following an open competition. The Technology Strategy Board is an executive body established by the Government to drive innovation. It promotes and invests in research, development and the exploitation of science, technology and new ideas for the benefit of business - increasing sustainable economic growth in the UK and improving quality of life. Finally, the authors would also like to acknowledge the financial support of Bombardier Aerospace Belfast.

References

[1]Saric, W. and Reed, H., "Toward Practical Laminar Flow Control," 2nd AIAA Flow Control Conference, AIAA, 2004.

[2]Atkin, C., "Laminar Flow Control: Leap or Creep?" 38th Fluid Dynamics Conference and Exhibit, AIAA, 2008.

[3]Mount, J. and Millman, V., "Development of an Active Laminar Flow Nacelle," AIAA, 21 st Joint Propulsion Conference, 1985.

[4]Vijgen, P., "An Industrial Perspective on Drag Reduction Technology and Implementation," Katnet II 2nd Drag-Reduction Workshop, Ascot, UK, KatnetII, 2008.

[5]Riordan, D., "Industrial Perspective - Bombardier Aerospace," Katnet II 2nd Drag-Reduction Workshop, Ascot, UK, KatnetII, 2008.

[6]Bouteiller, X., "Drag Reduction for Nacelle Applications," Katnet II 2nd Drag-Reduction Workshop, Ascot, UK, KatnetII, 2008.

[7]Younghans, J. and Lahti, D., "Experimental Studies on Natural Laminar Flow," 22nd Aerospace Sciences Meeting, AIAA, 1984.

[8]Radespiel, R., Horstmann, K. H., and Redeker, G., "Feasibility Study on the Design of a Laminar Flow Nacelle," *Journal of Aircraft*, 1990, pp. 959–965.

[9]Hastings, E., Schoenster, J., Obara, C., and Dodbele, S., "Flight Research on Natural Laminar," AIAA, AIAA/ASE/SAE/ASEE 22nd Joint Propulsion Conference, 1986.

[10]Riedel, H., Horstmann, K., Ronzheimer, A., and Sitzmann, M., "Aerodynamic Design of a Natural Laminar Flow Nacelle and the Design Validation by Flight Testing," *Aerospace Science and Technology*, 1998, pp. 1–12.

[11]Obara, C. and Holmes, B. J., "Flight-measured laminar boundary-layer-transition phenomena including stability theory analysis," Tech. rep., NASA, 1985, Technical Paper TP-2417.

[12]Lessen, M. and Gangwani, S. T., "Effect of small amplitude wall waviness upon the stability of the laminar boundary layer," *Physics of Fluids*, 1976, pp. 510–513.

[13]M.B. Bragg, M. K. and Cummings, M., "Airfoil Boundary Layer due to Large Leading-Edge Roughness," Aerospace Sciences Meeting and Exhibit, 33rd, Reno, NV, Jan 9-12, 1995, AIAA, 1995.

[14]Floryan, J. and Allman, U., "Flow over a leading edge with distributed roughness," *J. Fluid Mech.*, Vol. 216, 1990, pp. 629–656.

[15]Nitschke-Kowskpy, P. and Bippes, H., "Instability and transition of a three-dimensional boundary layer over a swept flat plate," *Phy. Fluids*, Vol. 786, 1988.

[16]Janke, E. and Balakumar, P., "Transition control using leading edge roughness," AIAA Fluid Dynamics Conference, 30th, Norfolk, VA, AIAA, 1999.

[17]W. Saric, R. C. and Reibert, M., "Leading-edge roughness as a transition control mechanism," Aerospace Sciences Meeting and Exhibit, 36th, Reno, NV, AIAA, 1998.

[18]Atkin, C., "Parametric Studies on the Application of Distributed Roughness Elements for Laminar Flow Control," 35th AIAA Fluid Dynamics Conference and Exhibit, Toronto, Ontario, AIAA, 2005.

[19]A. Carpenter, W. S. and Reed, H., "Laminar Flow Control on a Swept Wing with Distributed Roughness," 26th AIAA Applied Aerodynamics Conference, Honolulu, Hawaii, AIAA, 2008.

[20]Bearman, P. W., "Corrections for the effect of ambient temperature drift on hot-wire measurements on incompressible flows," Tech. rep., DISA Information No. 11, 1971.